Magnetic critical behavior in the $[Cu(1\text{-hydroxybenzotriazolate})_2(MeOH)]_n$ molecule-based random-field magnet

M. Fardis,[1,*] C. Christides,[1,2] G. Diamantopoulos,[1] V. Psycharis,[1] C. Raptopoulou,[1] V. Tangoulis,[3] and G. Papavassiliou[1]
[1]*Institute of Materials Science, National Center for Scientific Research "Demokritos," 15310 Athens, Greece*
[2]*Department of Engineering Sciences, School of Engineering, University of Patras, 26500 Patras, Greece*
[3]*Department of Materials Science, University of Patras, 26500 Patras, Greece*
(Received 10 July 2003; published 19 November 2003)

^{1}H nuclear-magnetic-resonance and magnetization measurements have been performed in the molecule-based solid $[Cu(btaO)_2(MeOH)]_n$ (btaOH stands for 1-hydroxybenzotriazolate) as a function of temperature. The compound exhibits a critical transition at $T_c = 5.7$ K from a high-temperature paramagnetic phase to a low-temperature magnetic phase characterized by relatively strong ferromagnetic interactions. The experimental results are best analyzed considering that the ground state of the system is a random-field ferromagnetic state in the absence of an external magnetic field. The dynamics of the electronic-spin fluctuations in the low-temperature magnetic phase are estimated using a two-level system model.

DOI: 10.1103/PhysRevB.68.184415 PACS number(s): 75.50.Xx, 76.60.−k, 33.25.+k

I. INTRODUCTION

Magnetism in molecule-based materials is a subject of continuing interest from both the fundamental and the technological point of view.[1] Of particular interest is the design of molecule-based ferromagnets that exhibit a spontaneous magnetization below a critical temperature T_c. The original synthetic route was based,[2] first, on the assembly of molecular bricks that form a low-dimensional system with a magnetic ground state and, second, on coupling the chains or layers in a ferromagnetic fashion. However, it is often difficult to realize the symmetry conditions that favor the parallel alignment of local spins in all dimensions. Thus, polymetallic-antiferromagnetically coupled or network-structured ferromagnetic, ferrimagnetic molecular structures were subsequently emerged.[3–6] In this context the reported ferromagneticlike behavior in a newly synthesized[7] $[Cu(btaO)_2(MeOH)]_n$ (btaOH stands for 1-hydroxybenzotriazole) homometallic polymeric complex deserves further examination. This complex crystallizes in a three-dimensional (3D) polymer motif with a structure built up with helices and exhibits bulk ferromagnetic properties below about 4 K.[7] It crystallizes in the tetragonal space group $P4_32_12$ with lattice parameters (at 25^0C) $a = 9.915(1)$ Å, $c = 14.715(2)$ Å. The Cu^{2+} ions display a square pyramidal coordination with four $btaO^-$ ligands on the basal plane and the oxygen of the disordered methanol molecule at the apical position [Fig. 1(a)]. Each $btaO^-$ ligand bridges two sequential metal ions through its oxygen O(1) and nitrogen N(3) atoms. Each Cu^{2+} ion is surrounded by four other coppers in a, slightly distorted, tetrahedral arrangement and is linked to them through the $btaO^-$ ligand. Through these bridging paths a 3D diamondlike lattice is formed [Fig. 1(b)].

Previous dc-magnetic-susceptibility measurements on a polycrystalline sample of $[Cu(btaO)_2(MeOH)]_n$ at $H_0 = 1000$ Oe have shown that the susceptibility follows the Curie-Weiss law with a Curie constant $C = 0.42$ emu K/mol and a positive paramagnetic Curie temperature $\theta_p = 8.35$ K, signifying the presence of ferromagnetic spin coupling among Cu ions.[7] In addition, ac-magnetic-susceptibility and dc-magnetization measurements[7] have revealed two inflection points which were tentatively attributed to two critical temperatures at 6.4 and 4.4 K. Although the exact physical origin of these transitions is ambiguous, it was suggested[7] that the two inflection points may reflect the observed anisotropy in the crystallographic axes. In view of the intriguing behavior of the magnetic data and of the fact that ferromagnetic insulators are relatively rare, it becomes evident that more sophisticated measurements are required to determine the magnetic state of $[Cu(btaO)_2(MeOH)]_n$. The aim of the present study is to probe the static and dynamic magnetic properties of this molecule-based solid by means of bulk magnetization measurements alongside ^{1}H pulsed nuclear-magnetic-resonance (NMR) experiments.

II. EXPERIMENTAL DETAILS

The synthesis and crystal structure of the $[Cu(btaO)_2(MeOH)]_n$ complex is described elsewhere.[7] ^{1}H pulsed NMR experiments were performed at 4.7 T using a Bruker MSL200 spectrometer operating at 200.145 MHz. An Oxford 1200CF continuous flow cryostat was employed for measurements in the range 3–300 K. At high temperatures, the ^{1}H NMR spectra were obtained by the Fourier transform of the nuclear free-induction decay at the Larmor frequency, since a single pulse of ~ 1.5–4 μsec was sufficiently strong to irradiate the whole NMR line. For low-temperature measurements, the spectra were obtained by the spin-echo point by point method while varying the frequency, because of the large width of the resonance line. T_1 spin-lattice and T_2 spin-spin relaxation times were measured using the standard spin-echo pulse sequence combined with the saturation recovery method for T_1 measurements. Dc-magnetic measurements were performed in a Quantum Design MPMSR2 superconducting quantum interference device magnetometer.

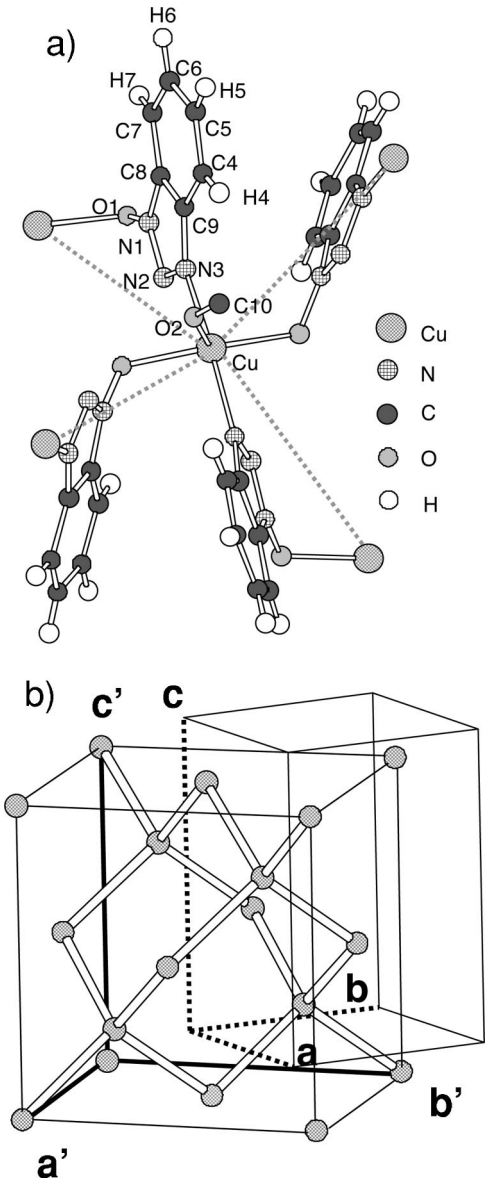

FIG. 1. (a) The square pyramidal coordination of Cu^{2+} is shown. The dotted lines indicate the tetrahedral arrangement of Cu ions. (b) The tetragonal supercell corresponding to the cubic cell of diamond. The original cell is also shown. The dimensions of the supercell are $a'=14.022$ Å and $c'=14.715$ Å. The a' axis is along the main diagonal of the base of the original cell.

III. RESULTS AND DISCUSSION

A. Magnetic measurements

1. Critical exponents from dc-susceptibility measurements

dc-susceptibility (χ) measurements are shown in Fig. 2 for three external fields $H=5$,50, and 1000 Oe between 3 and 10 K. No appreciable differences were observed between the field cooled and zero-field cooled curves down to 3 K. The strong divergence of χ indicates that there are fluctuations of large correlated domains of spins at about 6 K which can be assigned[7] to a magnetic critical temperature T_c. In the critical region of a ferromagnet there are[8] scaling equations

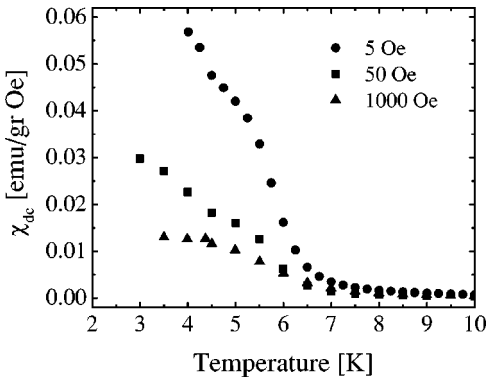

FIG. 2. dc-susceptibility measurements as a function of temperature for three applied fields.

for the magnetization $M(t,h)$: $M(t,h=0)\sim(-t)^{\beta}$ and $M(0,h)\sim h^{1/\delta}$, which are characterized by a set of critical exponents β and δ when the dimensionless variables $t=(T-T_c)/T$, $h=(g\mu_B H_{eff})/k_B T$, are introduced around the critical point T_c for an effective field H_{eff} between the cells in the correlated region $T\approx T_c$. The isothermal susceptibility can be calculated from $M(t,h)$ by means of $\chi=\partial M/\partial H$, and gives a[8] $\chi\sim(t)^{-\gamma}$, in small fields at temperatures just above T_c. Thus, log-log plots of the χ of a ferromagnet against $T-T_c$ should be linear with slope $-\gamma$, showing that χ diverges as $(T-T_c)^{-\gamma}$ in the critical region:

$$\chi\sim(T-T_c)^{-\gamma}. \tag{1}$$

In principle, a γ can be defined asymptotically close to T_c, as $t\to 0$. In this regime the static scaling hypothesis was put on firm theoretical ground and the renormalization-group analysis of the three-dimensional Heisenberg model[9] provides with high precision the critical exponents $\beta=0.3647(12)$, $\gamma=1.3866(12)$, which surpasses the experimentally available[8] precision of magnetic systems ($\beta\approx 0.37$, $\gamma\approx 1.33$, $\delta\approx 4$). The disagreement of critical exponents between theory and experiment is due, mainly, to the existence of long-range interactions in real systems. Kadanoff *et al.*[10] have estimated that the influence of these interactions on critical fluctuations in magnetization can be neglected if the extent of the critical region $|t|$ is

$$|t|\gg\left(\frac{g\mu_B S_{eff}M(0)}{k_B T_c}\right)^{1/\gamma}=t_c. \tag{2}$$

The estimated t_c for metallic ferromagnets (Fe, Ni, . . .) is of the order of 10^{-3}, indicating that the extent of the critical region must be at least of the order of 10^{-2}. However, there is no unambiguous way to determine the boundaries of the critical region from standard magnetic measurements and thus there is always a large uncertainty in the values of the critical exponents that are determined from such measurements. This problem can be faced by analyzing the experimental data in the nonasymptotic regime, far away from the critical region, where approach to criticality is described by nonuniversal effective critical exponents that are valid in a certain temperature interval.[11] To examine the tem-

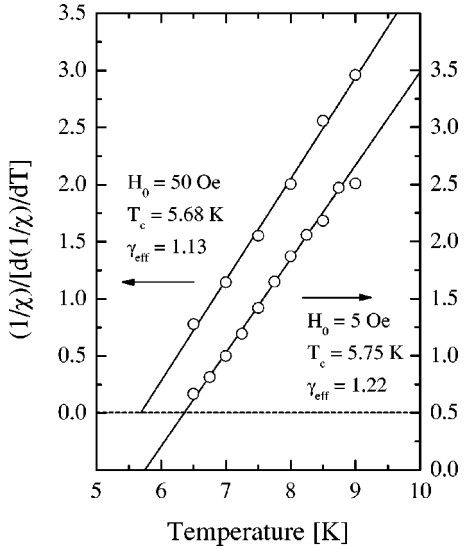

FIG. 3. Kouvel plots of the dc-susceptibility data. Open circles are the $(1/\chi)/[d(1/\chi)/dT]$ against T values that are calculated from the experimental data and solid lines are best-fit lines with slope $(1/\gamma_{eff})$ that intersect the T axis at T_c.

perature dependence of χ in the entire temperature range, Kouvel and Fisher[11] have introduced an effective exponent $\gamma_{eff}(t)$:

$$\gamma_{eff}(t) = \frac{d\ln\chi(t)}{d\ln t}. \tag{3}$$

In the asymptotic limit $(t \to 0)$ the effective and asymptotic exponents coincide. Thus, a plot of $(1/\chi)/[d(1/\chi)/dT]$ against T can give[11] a fit of the temperature dependence of the low field χ if we use Eqs. (1) and (3) just above the T_c. Equation (1) is expected to give a straight line with slope $(1/\gamma_{eff})$ that intersects the T axis at T_c. It is worth noting that this method avoids errors due to uncertainties[11,8] in T_c. In accordance, Fig. 3 shows that Eq. (1) fits well the susceptibility data (the curve for $H=1$ kOe is not shown for clarity) with a field-independent $T_c = 5.7 \pm 0.02$ K whereas the γ_{eff} is field and temperature range dependent, as expected for the nonasymptotic regime.

The obtained γ_{eff} values are between 1.1 and 1.25, whereas the Ginzberg-Landau theory predicts[8] a value of $\gamma = 1$ (Curie-Weiss law) far away from the critical region. These values are comparable with γ_{eff} values that were obtained[12] in amorphous magnets. Thus, as in amorphous ferromagnets,[13] the pertinent question here is the validity of the static scaling hypothesis for molecular ferromagnets since molecular and amorphous solids do not have a unique ferromagnetic ground state whereas there can be states with and without a net spontaneous magnetization which are very close in energy.

2. Arrot-like plots

High-field magnetic isotherms between 3 and 9 K are shown in Fig. 4. The temperature range between 4.4 K and 7.3 K was spanned with a resolution of 0.2 K. Complete

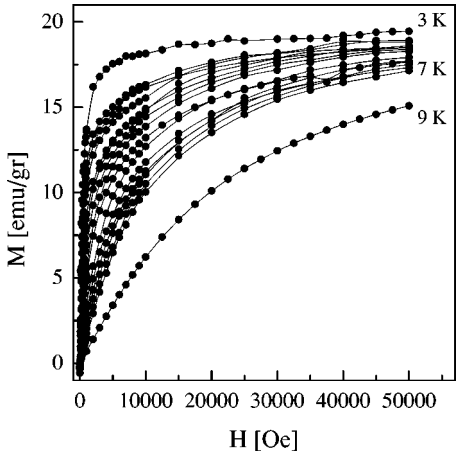

FIG. 4. High-field magnetic data.

saturation is achieved at 3 K in a field of about 2 T. Arrot plots,[14] where a set of isotherms of M^2 against H/M is plotted, are used as the decisive experimental method on whether a material is ferromagnetic or at least whether it possesses spontaneous net magnetization. However, the corresponding Arrot plots at low fields (Fig. 5) show no indication of spontaneous magnetization M_s. The isotherms never intercept the M^2 axis, confirming that $M_s = 0$ always intercept the H/M axis at a finite value, yielding a finite susceptibility and, therefore, no transition. This inconsistency, between magnetothermal (Figs. 2 and 3) and Arrot plot data (Fig. 5), comes from the basic concept behind the Arrot plots that relies on the Landau (mean-field) theory[8] of phase transitions. In Arrot's procedure, the intercept on the H/M axis is the $\chi^{-1} \sim t^{-\gamma}$ with $\gamma = 1$ and the critical isotherm is $H \sim M^{\delta}$ with $\delta = 3$. However, magnetic critical scattering experiments[8] show that the critical exponents γ and δ are closer to 1.3 and 4, respectively, indicating that the mean-field approximation is not correct in the critical region. Besides that, the data used for extrapolation back to $H/M = 0$ often come from substantial fields $H > 1$ kOe, which can alter the magnetic state of molecular or amorphous solids because they do not have a well defined ferromagnetic ground state.

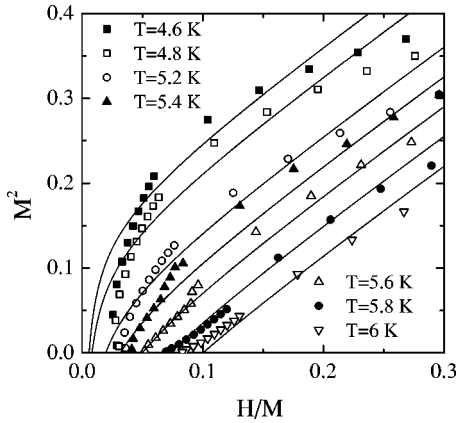

FIG. 5. Arrot-like plots between 4.6 and 6.0 K. Symbols are normalized experimental data and solid lines correspond to estimated curves from Eq. (4).

In the following we show that our data are more consistent with a random magnetic-field model. In this model, Aharony and Pytte[15] have solved the Ginzburg-Landau-Wilson Hamiltonian with a special random field, showing that the addition of higher-order or incompletely random-field terms in the calculated isotherms of M^2 as a function of H/M allow the appearance of a phase with a net magnetization, although the ground state has none (random-field magnet). These authors have shown that for dimensionalities $d<4$ the leading terms in the magnetic equation of state for Heisenberg-like models with random fields and random uniaxial anisotropies are given by

$$H/M = t + M^2 + A(m-1)(H/M)^{-\epsilon/2}, \tag{4}$$

where the T_c in t is the ordering temperature of the nonrandom problem, $\epsilon = 4-d$ is the *epsilon expansion*[16] about the effective system dimensionality of 4, and the units of M have been chosen to make the coefficient of M^2 equal to unity. In the random-field case $A = \alpha_F(\Delta/J)$, where the parameter Δ is a measure of the relative fluctuation strength[12] of the exchange interactions J. In this approximation, the family of the solid lines in Fig. 5 has been plotted according to Eq. (4), using the previously estimated value for the $T_c = 5.7$ K in t, an $A(m-1) = 0.015$, an $\epsilon = 1$, and properly normalized values of the magnetization data. Overall, the agreement between the calculated curves and the experimental data is satisfactory if someone considers that the model calculations have been carried out only to lowest order in Δ. An $\epsilon = 1$ for the exponent of the last term (H/M) in Eq. (4) gives a critical exponent[8] $\nu = 0.5 + (\epsilon/12) + O(\epsilon^2) = 0.58$ for the correlation length ξ, which is close to that expected for a three-dimensional Ising model. Generally, a three-dimensional Ising model describes magnetic systems with a uniaxial magnetic anisotropy. Such a uniaxial anisotropy may arise from the c' axis of the tetragonal supercell [Fig. 1(b)]. However, Eq. (4) needs higher-order terms in the case[15] of very large Δ or for data points close to the origin in Fig. 5. It is thus evident from the magnetization data (Fig. 4) that, although the magnetic susceptibility diverges (Fig. 2) at a finite temperature T_c, there is no long-range order (the magnetization M goes to zero with the field H) at any finite temperature T, as expected from a random-field magnet.[15] Thus ^{1}H NMR spectroscopy was used to probe the thermal evolution of local magnetic interactions in this system.

B. NMR measurements

1. Line shapes and T_2 spin-spin relaxation time

^{1}H NMR spectra for $[Cu(btaO)_2(MeOH)]_n$ in a powder sample were acquired as a function of temperature at applied magnetic field $H_0 = 4.7$ T. Figure 6 shows typical ^{1}H NMR spectra for selected low temperatures near and above the transition temperature T_c.

The high-temperature spectra (not shown) are narrow with a width in the kilohertz range, whereas the low-temperature spectra below 60 K are broadened with a width in the megahertz range. The low-temperature spectra have been fitted with a Voigt line-shape function that takes into account Gaussian broadening (solid lines in Fig. 6). In a paramagnet, the shape, width, and the shift of the NMR line are determined by the local field at the resonating nuclei. Apparently there is no appreciable frequency shift of the peak from the γH_0 value as a function of temperature, indicating that the relaxation mechanism between the electronic spin and the ^{1}H nuclei is predominantly of dipolar origin.[17]

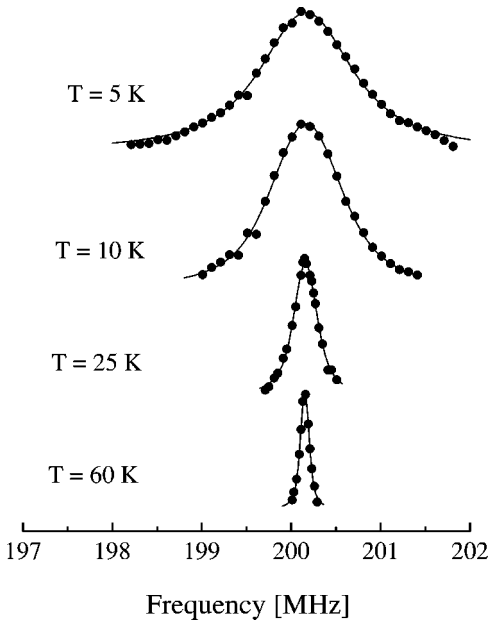

FIG. 6. ^{1}H NMR spectra at selected low temperatures.

Figure 7 shows the obtained full width at half maximum ΔH (circles) as a function of temperature, scaled with the magnetization data (solid line) that were acquired at the same field $H_0 = 4.7$ T. The dashed line is a Curie-Weiss law $[\chi \propto (T-\vartheta_p)^{-1}]$, with the paramagnetic Curie temperature[7] $\theta_p = 8.4$ K. The T_2 spin-spin relaxation time (triangles in Fig. 7) scales also with ΔH in this temperature region. These results show clearly that the probed contributions from the local magnetic interactions are proportional to bulk magne-

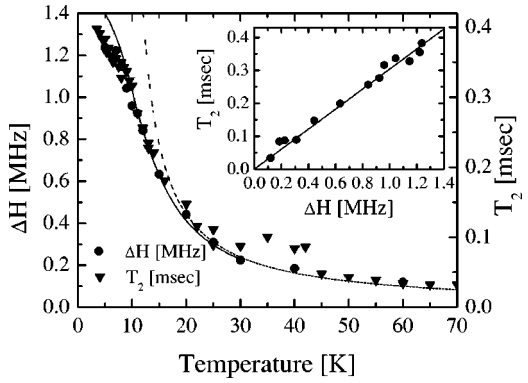

FIG. 7. ^{1}H NMR linewidth ΔH (circles) and T_2 (triangles) spin-spin relaxation time as a function of temperature. The solid line shows the magnetization data that were acquired at the same field $H_0 = 4.7$ T with NMR data. The dashed line shows a Curie-Weiss law $[\chi \propto (T-\vartheta_p)^{-1}]$, with a $\theta_p = 8.4$ K. The inset shows the linear relationship between T_2 and ΔH.

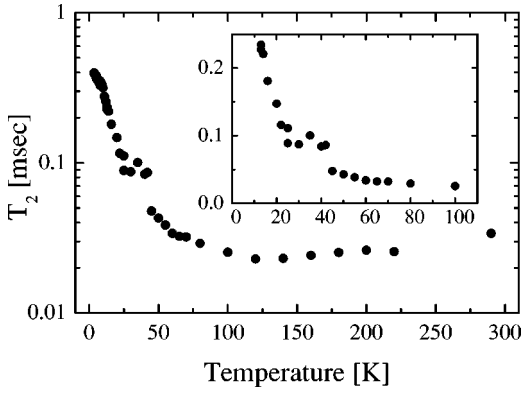

FIG. 8. T_2 spin-spin relaxation time as a function of temperature. The inset shows in detail the local maximum of T_2 observed between 30 and 45 K.

tization or to χH_0.[18] The broadening of the NMR line shows a significant distribution of paramagnetic shifts at the nuclear site, since in such a case, the resonance field would be distributed over a range ΔH given by[19,20] $\Delta H = 3\alpha_{\rm lat}\chi H_0$, with $\alpha_{\rm lat}$ being a characteristic constant of the crystal lattice. The experimental width is determined by superposing a symmetric broadening over this distribution. Such a distribution may result from a variation in electronic structure among sites, variations in demagnetizing fields among differently shaped grains in a powdered sample, or from anisotropy of the shift in a randomly oriented powder.[21]

Figure 8 shows the spin-spin relaxation time T_2 as a function of temperature for a $H_0 = 4.7$ T between 5 and 300 K. In principle, this relaxation time is a measure of the homogeneously broadened NMR line. As seen in Fig. 8 the T_2 is approximately constant above 100 K because it is mainly determined by the dipolar interactions between the protons in the btaO^- ligands. In this temperature range the decay of relaxation could be analyzed as the sum of two exponentials. Specifically, the nonexponential character of this relaxation time is due to the five nonequivalent proton sites: H4, H5, H6, H7, and H10 (attached to C10 in Fig. 1) in the unit-cell volume [Fig. 1(a)]. Below 100 K the T_2 increases progressively and exhibits both an exponential relaxation decay and a wide T_2 maximum between 30 and 45 K (inset of Fig. 8). This maximum is reproducible in repeatable NMR measurements and thus is a real experimental feature. Since there is no detectable anomaly in bulk magnetic measurements above 10 K then, as will be explained below, the origin of the T_2 maximum can be related to the detuning effects that occur below 60 K (Fig. 7). In addition, the observed increase of T_2 with decreasing temperature in the region well above the T_c (5.7 K) is quite unusual for a paramagnet and cannot be explained with the temperature-independent nuclear dipole-dipole relaxation mechanism in the rigid-lattice approximation. Since this increase of T_2 occurs well above the macroscopic T_c (Fig. 2) and, in addition, the observed relaxation time T_1 (see below) is temperature independent in that region, then such a strong temperature dependence of T_2 cannot be related to the onset of short-range ferromagnetic interactions on cooling.

The inset in Fig. 7 reveals a linear relationship between T_2 and ΔH below 60 K, signifying an unexpected correlation between the rates of increase of T_2 and ΔH. Since, usually, T_2 shortens as ΔH increases then the observed proportionality $T_2 \sim \Delta H$ below 60 K suggests that T_2 is also subjected to the inhomogeneity of the local electronic moments. These results are consistent with the model[22] of *microscopic* inhomogeneous broadening of the resonance-frequency (or local-field) distribution. Such inhomogeneities may result from nonmagnetic impurities or strains in the lattice[22,23] and can separate (detune) the resonant frequencies of a pair of nuclear spins to such an extent as to strongly inhibit mutual spin flips. This kind of inhomogeneities prevents mutual spin flips of the nuclei due to nonconservation of energy if the difference in their Zeeman energies is larger than the strength of the interaction between them. Thus, the reduction in the number of allowed transitions due to detuning can lead to a longer transverse relaxation time T_2, where according to the model, the shape of the relaxation decay could be a single exponential[22] or a sum of exponentials[23] depending on the exact form of the inhomogeneous broadening. In accordance, the results in Fig. 8 are consistent with a single-exponential relaxation decay between 5 and 180 K. The temperature dependence of T_2 near the critical region is discussed in Sec. III C in connection with the spin-lattice relaxation time.

2. T_1 spin-lattice relaxation time

Nuclear T_1 measurements determine the intensity and correlation times of magnetic and lattice fluctuations. Thus, the low-frequency spin dynamics of the electronic system can be explored in paramagnets and magnetically ordered systems. The relaxation rates are caused by the time dependence of the fluctuating local magnetic fields, which, in the system examined here, originates from the fluctuations of the localized Cu-ion electron moment. The spin-lattice relaxation time is related to the electron spin-spin correlation function via

$$\frac{1}{T_1} \propto \int dt \cos(\omega_0 t)\langle h(t)h(0)\rangle, \tag{5}$$

where ω_0 is the NMR frequency and $h(t)$ is the fluctuating field due to the electron spin. The analysis of the NMR line shapes (Figs. 6–8) has shown that the electronic spins of Cu are coupled with the ^{1}H nuclei through the nuclear-electron dipolar interactions.

The ^{1}H spin-lattice relaxation time T_1 of $[\mathrm{Cu(btaO)_2(MeOH)}]_n$ was measured at a frequency of 200.145 MHz (4.7 T) between room and liquid-helium temperatures and is shown in Fig. 9. The relaxation recoveries were nonexponential functions due to the many nonequivalent nuclear sites [Fig. 1(a)] and could be analyzed using the well-known ''stretched'' exponential function $\exp(-t/T_1)^{\alpha}$ where $0<\alpha<1$. Figure 10 shows the stretched exponent α as a function of temperature. Figure 9 shows that the T_1 relaxation time is temperature independent between 50 and 300 K whereas it remains field (or frequency) independent over a quite considerable frequency range at higher tempera-

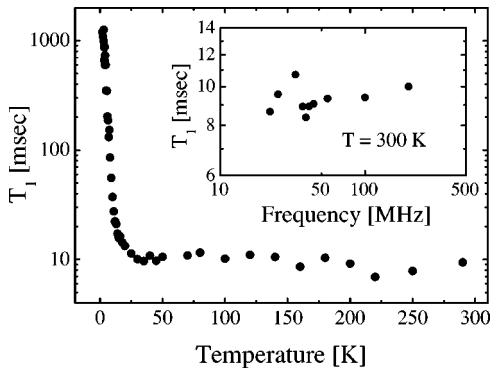

FIG. 9. T_1 spin-lattice relaxation time as a function of temperature. In the inset the frequency dependence of T_1 is shown at 300 K.

tures (inset of Fig. 9). These results indicate that the high-temperature approximation of Moriya's[24] calculation can be readily applied.

Moriya,[24] in his pioneering work, expressed the nuclear relaxation rate caused by the hyperfine coupling between the electron spin and the nuclear spin in exchange-coupled paramagnets in terms of autocorrelation function of the electron spins. In his calculation he neglected the correlation between the different electron spins in the high-temperature approximation. The expression for T_1 and T_2 thus obtained showed no appreciable temperature dependence. Assuming a Gaussian distribution centered at zero frequency of the local-field

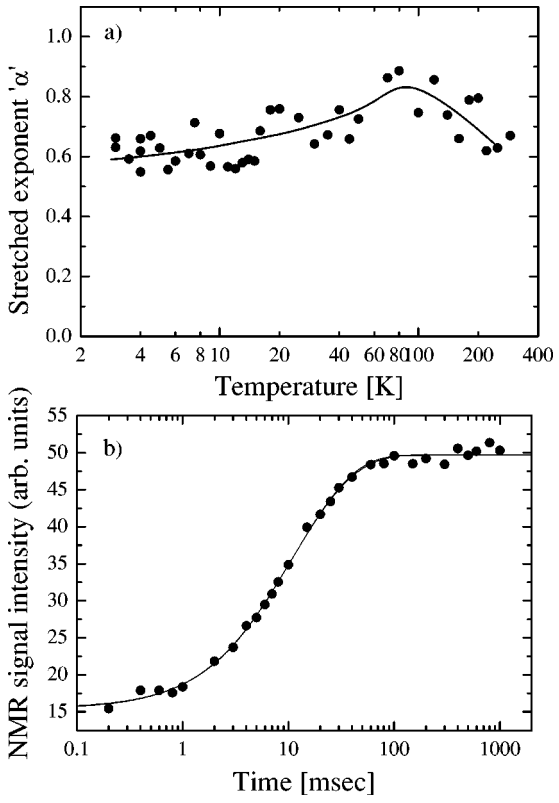

FIG. 10. (a) "Stretched" exponent α as a function of temperature. The solid line is an "eyeball" fit to the data and (b) T_1 relaxation recovery (circles). There are two indistinguishable fitting lines through the data, as described in the text.

spectra at the nucleus due to the fluctuating electronic spins, Moriya's result in the high-temperature region is given by[24]

$$\frac{1}{T_1}=\frac{2\sqrt{2\pi}}{3}\frac{\gamma_e^2\gamma_n^2\hbar^2}{\omega_e}S(S+1)\sum_j\frac{f(\alpha\beta\gamma)}{r_j^6}, \tag{6}$$

where γ_e, γ_n are the electron and nuclear gyromagnetic ratios, respectively, $S=1/2$, $f(\alpha\beta\gamma)$ is a geometrical factor, of the order of unity, which depends on the directional cosines of r_j connecting the given nuclear site (protons) to the jth magnetic ion (copper) with respect to the quantization axis,[24] and ω_e is the exchange frequency of the electron moments given by

$$\omega_e^2=\frac{8}{3}\left[\frac{J}{\hbar}\right]^2 zS(S+1), \tag{7}$$

where J is the effective exchange-coupling constant that results from the atomic spin density on neighboring atoms and z is the number of nearest neighbors.

An estimation of T_1 can be made from Eq. (6), assuming the positions of the five nonequivalent proton sites from the unit cell shown in Fig. 1(a). First we calculate the geometrical factor in Eq. (6). The calculation of the sum $\Sigma_j 1/r_j^6$, for each of the five protons in the unit cell over a sphere of radius up to 11 Å gives values between 3.1×10^{44} and 1.5×10^{45} cm^{-6}. Such a wide range of distances can be considered responsible for the observed stretched exponential decay of T_1 in Fig. 10. To obtain the mean value of T_1 we need the mean value for the sums of the five proton sites which, assuming[24] an $f(\alpha\beta\gamma)=1$, gives $\Sigma_j f(\alpha\beta\gamma)/r_j^6=7.9\times10^{44}$ cm^{-6}. In addition, an estimation of ω_e can be made from Eq. (7) by considering a *kinetic exchange interaction* only between the four copper nearest neighbors in Fig. 1 [$z=4$ in Eq. (7)]. An effective coupling constant J [Eq. (7)] can be estimated from the observed $T_c=5.7$ K if the expression obtained by Rushbrooke and Wood[25] is used:

$$\frac{kT_c}{J}=\frac{5}{96}(z-1)[11S(S+1)-1]. \tag{8}$$

These relations give a $J/k_B=5.0$ K and a $\omega_e=1.9\times10^{12}$ sec^{-1}. Thus, considering (i) the averaging procedure we have undertaken, (ii) the stretched exponential character of the experimental decays, and (iii) the uncertainty in the value of the geometrical factor, Eq. (6) gives a $T_1=8$ msec that fits extremely well with the experimental T_1 values shown in the high-temperature region of Fig. 9.

So far, we have successfully calculated the average relaxation time T_1 for the higher-temperature (paramagnetic) region. In addition, we will show that we can fully reconstruct the experimental decay curves without additional adjustable parameters, by considering only five individual relaxation times for each proton site. In other words, we will show that it is possible to simulate the stretched exponential decay of T_1 by the sum of the calculated relaxation times. The sums for the five proton sites and the corresponding T_1 values from Eq. (6) are given in Table I.

TABLE I. Calculated T_1 relaxation times and geometrical sums for the five inequivalent proton sites in the unit cell, according to Eq. (6).

^{1}H site	$\Sigma_j \frac{1}{r_j^6}(\mathrm{cm}^{-6})$	T_1 (msec)
H4	1.499×10^{45}	4.0
H10	8.627×10^{44}	7.0
H7	7.184×10^{44}	8.4
H5	5.650×10^{44}	10.7
H6	3.094×10^{44}	19.5

To fit the wide range of experimental T_1 values (circles) in Fig. 10(b) we have chosen from Table I three representative relaxation times of 4, 8, and 20 msec in order to form a three-exponential recovery fitting function. In this procedure, the relaxation times were fixed and their weights were the adjustable parameters. The best-fitting curve is shown in Fig. 10(b), together with the stretched exponential fit (both shown as solid lines). Remarkably, the two fitting curves coincide and the fit to the experimental points is excellent. Thus, despite the difficulties associated with many nonequivalent proton sites, the good agreement between the experimental data and the calculated values from the simple model used shows that a better than order of magnitude estimate for the J and ω_e values has been achieved from the high-temperature (paramagnetic) region of T_1.

C. NMR relaxation rates in the critical region

The high-temperature approximation, where pair correlation between the different electron spins is neglected, is no longer valid at finite temperatures and especially around the critical temperature. In this region, the experimental $1/T_1$ and $1/T_2$ relaxation rates are shown in Figs. 11(a) and 11(b) as a function of temperature. As seen, the high-temperature approximation does not apply below 30 K, where the $1/T_1$ decreases by approximately two orders of magnitude. In spite of years of theoretical effort, the problem of calculating correlation functions at finite temperatures, in order for Eq. (5) to be applicable, has not yet been solved. Moriya[26] has managed to correlate the temperature variation of the NMR relaxation times with the temperature dependence of the wave-vector-dependent susceptibility. In addition, various interpolation procedures, which combine moment expansions at short times and diffusive decay at long times, have been particularly successful.[27]

In this section we demonstrate that a simple model that is based on a two-level scheme[28] for the fluctuations of the orientation of the magnetic moment is adequate to describe our T_1 relaxation data close to and above the transition temperature. This model has been originally proposed by Hardeman *et al.*[28] and it was frequently employed for the nuclear-magnetic relaxation in paramagnets.[18,29,30]

The main assumption of the model is that during a certain average lifetime τ_1 the magnetic moment in a Cu ion is directed parallel to the time average magnetization $\langle M\rangle$

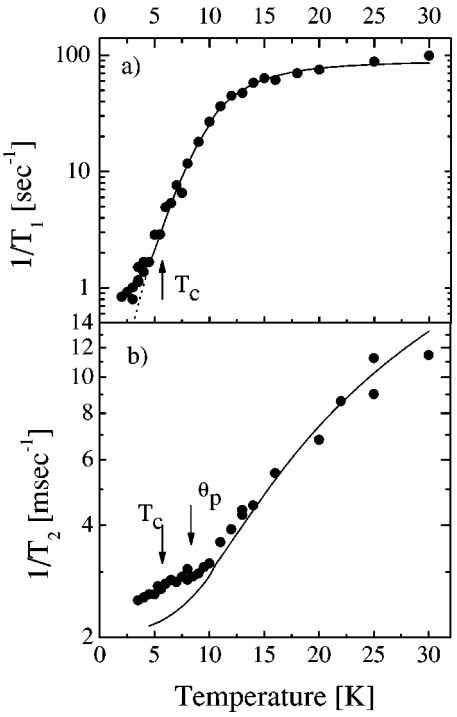

FIG. 11. $1/T_1$ (a) and $1/T_2$ (b) relaxation rates as a function of temperature in the low-temperature region. The solid line in (a) is a fit to Eq. (11) and the solid line in (b) is inverse magnetization data.

whereas during an average lifetime τ_2 is antiparallel to it. Thus, the time-average magnetization is given by

$$\langle M\rangle = M_s\left(\frac{\tau_1-\tau_2}{\tau_1+\tau_2}\right), \tag{9}$$

where M_s is the saturation magnetization. Accordingly, the magnetic local field at the proton site h_i has the same time dependence as the magnetic moment of the nearest Cu ion and its average value is proportional to the average value of the magnetic moment, following Eq. (9). In this approximation, the spectral density $J(\omega)$ is given by[28]

$$J(\omega) = h_{i0}^2 \frac{8\tau_1\tau_2}{(\tau_1+\tau_2)^2}\frac{\tau}{(1+\omega^2\tau^2)}, \tag{10}$$

where $1/\tau = 1/\tau_1 + 1/\tau_2$, h_{i0} is the saturation value of h_i at $T=0$, and ω is the Larmor angular frequency. For the intensity at the Larmor frequency of the proton, the approximation $\omega\tau \ll 1$ could be applied, and after some algebra the relaxation rate $1/T_1 \sim J(\omega)$ can be expressed in terms of $\langle M\rangle$ by using Eq. (9):

$$\frac{1}{T_1} = \frac{\gamma_n^2 h_{i0}^2}{4}\left(\frac{M_s^2-\langle M\rangle^2}{M_s^2}\right)^2(\tau_1+\tau_2). \tag{11}$$

The interesting feature of Eq. (11) is that $1/T_1$ is proportional to both the sum $(\tau_1+\tau_2)$ and the reduced magnetization: $(1-\langle M\rangle^2/M_s^2)^2$ term deduced easily from typical magnetization versus temperature measurements. The temperature dependence of $\langle M\rangle$ has been measured (solid

line in Fig. 7) and following an estimation of the saturation magnetization, the $1/T_1$ NMR relaxation data have been fit to Eq. (11) and the result is shown as solid line in Fig. 11(a). The fit is excellent between 5 and 30 K, indicating the validity of this two-level, microscopic model for temperatures close to and above the T_c. The good fits in Fig. 11 indicate that the $(\tau_1+\tau_2)$ sum can have a constant value in that region. In addition, Eqs. (6) and (11) should become identical in the high-temperature (paramagnetic) region, where the $(1-\langle M\rangle^2/M_s^2)^2$ term tends to 1. In this limit, the value of $(\tau_1+\tau_2)$ is given by $1/\omega_e \simeq 5\times 10^{-13}$ sec^{-1}. Below the $T_c = 5.7$ K, the experimental data deviate from the fitting curve of Eq. (11) and the dotted line in Fig. 11(a) is an extrapolation of the reduced magnetization data below 5 K. This deviation is not unexpected because there is no reason for the $(\tau_1+\tau_2)$ sum to be constant below the T_c. Despite this small deviation, no critical slowing down of the spin fluctuations has been observed in the $1/T_1$ NMR data near the transition temperature. This is due to the smearing effect of the large ($\simeq$4.7 T) applied magnetic field, since $(g\mu_B H \sim k_B T)$. Generally, the application of a magnetic field suppresses the critical fluctuations and reduces the characteristic lifetimes.[31] A more abrupt change in the NMR data near the critical point is observed in the temperature dependence of $1/T_2$. It shows that, despite the external application of 4.7 T, the $1/T_2$ [circles in Fig. 11(b)] is more sensitive to the paramagnetic Curie point $\theta_p = 8.35$ K than the inverse magnetization data [solid line in Fig. 11(b)].

IV. CONCLUSIONS

In summary, a complete set of magnetization-temperature-field and NMR measurements have been performed in the molecule-based material $[\mathrm{Cu(btaO)_2(MeOH)}]_n$. The successful analysis of M^2 versus H/M plots in Fig. 5 with a magnetic equation of state [Eq. (4)], which assumes a random-field ground state for the $[\mathrm{Cu(btaO)_2(MeOH)}]_n$ material, can explain the absence of remanent magnetization (at $H=0$ Oe) from the M-H curves below the observed $T_c = 5.7$ K. In support, using the expressions of Rushbrooke and Wood,[25] the magnitude of the exchange interactions and the spin fluctuations in the paramagnetic state obtained from proton-NMR data are consistent with the observed transition temperature. In addition, the proton NMR relaxation data have been successfully analyzed near the critical region in terms of a microscopic two-level scheme model that assumes[28] electronic-spin fluctuations in Cu. The magnetic susceptibility diverges strongly at a finite temperature. The analysis of $(1/\chi)/[d(1/\chi)/dT]$ against T gives a critical temperature of 5.7 K and a nonuniversal critical exponent γ_{eff} that is between 1.1 and 1.2. A similar susceptibility critical exponent $\gamma = 1.22(2)$ has been observed[32] in the organic ferromagnet tetrakis(dimethylamino)ethylene-C_{60} (TDAE-C_{60}) as well. In both systems, the $[\mathrm{Cu(btaO)_2(MeOH)}]_n$ and the[32] TDAE-C_{60}, the measured critical exponents differ significantly from the ones of the 3D Heisenberg model. In the case of TDAE-C_{60}, the observed violation of the hyperscaling relations is due to a reduced effective dimension, indicating that the fluctuations at the critical transition ($T_c = 16.1$ K) are stronger than purely thermal fluctuations. Such an enhancement of fluctuations may arise from the configurational disorder in random-field systems,[33] which for[32] TDAE-C_{60} results in critical exponent values[32] that are closer to calculated exponents for the random-exchange Ising model.[34] In the system examined herein, macroscopic magnetic and microscopic NMR measurements suggest that the observed susceptibility critical exponents are closer to calculated exponents for the random-exchange Ising model,[34] indicating that the $[\mathrm{Cu(btaO)_2(MeOH)}]_n$ material exhibits the characteristic fluctuations of random-field systems at the critical region. In the near future, NMR experiments at low magnetic fields are planned in order to explore in detail the slowing down of the spin fluctuations around the critical region.

ACKNOWLEDGMENT

We wish to thank Professor S. Perlepes from University of Patras for providing the samples.

*Electronic address: mfardis@ims.demokritos.gr

[1] J.S. Miller, Inorg. Chem. **39**, 4392 (2000), and references therein.
[2] J.S. Miller, J.C. Calabrese, H. Rommelmann, S.R. Chittipeddi, J.H. Zhang, W.M. Reiff, and A.J. Epstein, J. Am. Chem. Soc. **109**, 769 (1987).
[3] J.M. Manriquez, G.T. Yee, R.S. McLean, A.J. Epstein, and J.S. Miller, Science **252**, 1415 (1991).
[4] T. Mallah, S. Thiébaut, M. Verdaguer, and P. Veillet, Science **262**, 1554 (1993).
[5] Ø. Hatlevik, W.E. Buschmann, J. Zhang, J.L. Manson, and J.S. Miller, Adv. Mater. (Weinheim, Ger.) **11**, 914 (1999).
[6] S.D. Holmes and G. Girolami, J. Am. Chem. Soc. **121**, 5593 (1999).
[7] V. Tangoulis, C.P. Raptopoulou, V. Psycharis, A. Terzis, K. Skorda, S. Perlepes, O. Cador, O. Kahn, and E.G. Bakalbassis, Inorg. Chem. **39**, 2522 (2000).
[8] M.F. Collins, *Magnetic Critical Scattering* (Oxford University Press, Oxford, 1989).
[9] J.C. LeGuillou and J. Zinn-Justin, Phys. Rev. Lett. **39**, 95 (1975).
[10] L.P. Kadanoff, W. Götze, D. Hamblen, R. Hecht, E.A.S. Lewis, V.V. Palciauskas, M. Rayl, J. Swift, D. Aspnes, and J. Kane, Rev. Mod. Phys. **39**, 395 (1967).
[11] J.S. Kouvel and M.E. Fisher, Phys. Rev. **136**, A1626 (1964).
[12] M. Fähnle, G. Herzer, H. Kronmüller, R. Meyer, M. Saile, and T. Egami, J. Magn. Magn. Mater. **38**, 240 (1983).
[13] K. Moorjani and J.M.D. Coey, *Magnetic Glasses* (Elsevier, Amsterdam, 1984).
[14] A. Arrot, Phys. Rev. **108**, 1394 (1957).
[15] A. Aharony and E. Pytte, Phys. Rev. Lett. **45**, 1583 (1980).
[16] K.G. Wilson and M.E. Fisher, Phys. Rev. Lett. **28**, 240 (1972).
[17] E.A. Turov and M.P. Petrov, *Nuclear Magnetic Resonance in Ferro-and Antiferromagnets* (Wiley, New York, 1972).
[18] M. Fardis, G. Diamantopoulos, M. Karayianni, G. Papavassiliou, V. Tangoulis, and A. Konsta, Phys. Rev. B **65**, 014412 (2001).
[19] E.D. Jones, Phys. Rev. **180**, 455 (1969).
[20] L.E. Drain, Proc. Phys. Soc. London **80**, 1380 (1962).

[21] K.E. Sakaie, C.P. Slichter, P. Lin, M. Jaime, and M.B. Salamon, Phys. Rev. B **59**, 9382 (1999).
[22] D. Hone, V. Jaccarino, T. Ngwe, and P. Pincus, Phys. Rev. **186**, 291 (1969).
[23] J. Barak, I. Siegelstein, A. Gabai, and N. Kaplan, Phys. Rev. B **8**, 5282 (1973).
[24] T. Moriya, Prog. Theor. Phys. **16**, 23 (1956).
[25] G.S. Rushbrooke and P.J. Wood, Mol. Phys. **1**, 257 (1958).
[26] T. Moriya, Prog. Theor. Phys. **28**, 371 (1962).
[27] F. Borsa and M. Mali, Phys. Rev. B **9**, 2215 (1974).
[28] G.E.G. Hardeman, N.J. Poulis, and W.v.D. Lugt, Physica (Utrecht) **22**, 48 (1956).
[29] T. Kohmoto, T. Goto, S. Maegawa, N. Fujiwara, Y. Fukuda, M. Kunitomo, and M. Mekata, Phys. Rev. B **49**, 6028 (1994).
[30] T. Goto, T. Koshiba, T. Kubo, and K. Agawa, Phys. Rev. B **67**, 104408 (2003).
[31] M.C. Chen and C.P. Slichter, Phys. Rev. B **27**, 278 (1983).
[32] A. Omerzu, M. Tokumoto, B. Tadic, and D. Mihailovic, Phys. Rev. Lett. **87**, 177205 (2001).
[33] W. Kleemann, Int. J. Mod. Phys. B **7**, 2469 (1993).
[34] H.G. Ballesteros, L.A. Fernandez, V. Martin-Mayor, A. Munoz-Sudupe, G. Parisi, and J.J. Ruiz-Lorenzo, Phys. Rev. B **58**, 2740 (1998).